energies

MDPI

Article

Research on IPFC-Based Dynamic Droop Control Strategy

Chaofan Ding [1], Xiaopeng Li [2,3], Baohong Li [1,*], Qin Jiang [1], Menghao Wen [1] and Tianqi Liu [1]

[1] College of Electrical Engineering, Sichuan University, Chengdu 610065, China; dingchaofan@stu.scu.edu.cn (C.D.); jiangqin_jq@126.com (Q.J.); 2020141440339@stu.scu.edu.cn (M.W.)
[2] Power Internet of Things Key Laboratory of Sichuan Province, Chengdu 610072, China; lxpbsd@163.com
[3] State Grid Sichuan Electric Power Research Institute, Chengdu 610041, China
* Correspondence: scu_lbh@163.com

Abstract: The interline power flow controller (IPFC) presents a promising solution for managing the directional and quantitative interaction of power between different lines, facilitating a significant improvement in power system stability. Based on such a background, this paper proposes a dynamic droop control strategy to improve frequency stability through the use of IPFC equipment. To enhance the active power support ability of the IPFC, additional frequency control for the IPFC's active power control loop is designed with droop control, where each IPFC's power flow control limitations are also considered to make sure the original power of each line is controllable. Besides the addition of such basic control, the proposed droop strategy is designed in a dynamic style. The droop coefficients of each IPFC can be varied according to each line's power transmission margin, such that the power fluctuations can be shared more reasonably based on such a dynamic droop coordination strategy. The proposed methods are verified through PSCAD simulations. The results show that the dynamic droop control cannot only suppress the frequency disturbance, but also make power dispatch more efficient.

Keywords: IPFC; droop control; frequency stability; dynamic control

Citation: Ding, C.; Li, X.; Li, B.; Jiang, Q.; Wen, M.; Liu, T. Research on IPFC-Based Dynamic Droop Control Strategy. *Energies* **2023**, *16*, 5400. https://doi.org/10.3390/en16145400

Academic Editors: Fabio Crescimbini and Marco Di Benedetto

Received: 12 June 2023
Revised: 7 July 2023
Accepted: 13 July 2023
Published: 15 July 2023

1. Introduction

With economic development, the geographical gap between power supply and load has increased. Additionally, the influx of new energy has resulted in power system development aimed toward long-distance, large-capacity and cross-regional networking transmission modes. Consequently, the structure of transmission networks has become increasingly complex, while operation modes have diversified. This scenario has led to the intertwining of several issues, such as power oscillations and the uneven distribution of network power flows. Furthermore, the advancement of novel energy sources and the increased utilization of power electronic components has posed significant power quality challenges for the power grid, including issues such as voltage dips and swells, flickers and an imbalanced voltage [1,2]. These problems pose new challenges to the power grid's safe and reliable operation [3–5]. Nonetheless, flexible AC transmission system (FACTS) technology can effectively address these challenges. FACTS technology is a new technology that leverages power electronics technology and control technology to a flexibly control AC transmission. Without altering the grid structure, the FACTS can swiftly adjust the transmission line parameters and accurately regulate the system power flow in real-time to enhance the power grid's security. As such, FACTS technology has a wide application prospect in an increasingly complex power system.

Third-generation flexible AC transmission system (FACTS) devices, namely, the interline power flow controller (IPFC) and the unified power flow controller (UPFC), have gained significant attention in recent times [6]. The UPFC, owing to its exceptional line power flow control capability, has been utilized in practical engineering, leading to an improvement in power flow distribution and the voltage stability of power systems [7,8].

On the other hand, unlike the UPFC, the IPFC has the ability to control the power flow of multiple lines at the same time, apart from regulating the power flow on installed lines, so as to reduce the risk of the power flow exceeding the limit on heavy-load lines [9]. This unique characteristic makes the IPFC a more powerful and versatile power flow control device. Current research on the IPFC has focused on low-frequency oscillation suppression, a location and constant volume strategy and power flow optimization, among other aspects. However, despite the growing interest in the IPFC, there is a lack of information about its participation in frequency regulation and the improvement of the system's stability.

In a voltage-source-converter (VSC)-based multiterminal flexible direct current transmission (VSC-MTDC) system, droop control serves as a coordinated control method between converter stations that can achieve both fast power distribution and DC voltage control. In the event of an AC system failure, a frequency adjustment is reliant on the frequency modulation capability of the fault AC system itself [10]. To overcome this limitation, reference [11] proposed introducing a frequency outer loop output into the droop control power reference value of converter stations, enabling the converter stations to participate in system frequency adjustments. Additionally, reference [12] adjusted the frequency through interstation communication by utilizing the frequency difference between different AC systems. References [13,14] further enhanced this approach by combining additional frequency control with virtual synchronous control technology to control frequency deviations and frequency change rates, thereby providing frequency adjustments to multiterminal flexible DC transmission systems. By incorporating frequency control into the control strategy, the VSC-MTDC system can assist the AC/DC hybrid system in maintaining frequency stability, providing a reference for AC systems with IPFCs to enhance system stability by absorbing unbalanced power through the IPFC.

According to the above description, it could be seen that IPFC studies usually focus on its power flow control strategies. However, the additional frequency control of the IPFC is lacks in research. To solve such a problem, this paper proposes a dynamic droop control for the IPFC. The novelty of the proposed method can be described as follow:

(1) An additional frequency control is introduced into the IPFC control loop, such that the IPFC cannot only control the steady-state power flow on its line, but can also increase the frequency stability of the AC system in transient disturbances.
(2) Droop control is used when designing the IPFC's additional frequency control. Hence, the frequency controllability of the IPFC can be efficiently adjusted, and the control characteristic of the IPFC is clear and similar to AC generators.
(3) To make sure the controlled lines operate in transmission limitations, dynamic droop coefficients are also proposed to adjust the additional frequency controllability.

The model established in PSCAD/EMTDC software verifies the effectiveness of the proposed dynamic droop control in different conditions, including line power changes, load variations and wind power fluctuation conditions.

2. The Mechanism of the IPFC

The diagram presented in Figure 1 depicts the fundamental configuration of the IIPFC for N lines. This system comprises various voltage source converters (VSCs), which are arranged in a back-to-back configuration and are linked through a shared DC bus. Each converter is connected to a particular line via a series transformers. To regulate the power flow, the converter injects a voltage component with a controllable amplitude and phase angle into the line, with the initial voltage of the line, altering the line's parameters and, consequently, changing the power flow distribution in the line. Thus, the line that contains the IPFC can be considered a high-impedance power supply, capable of acquiring or injecting active and reactive power to other areas of the power system. This approach effectively balances the power flow of each transmission line and enhances the transmission capacity of the system.

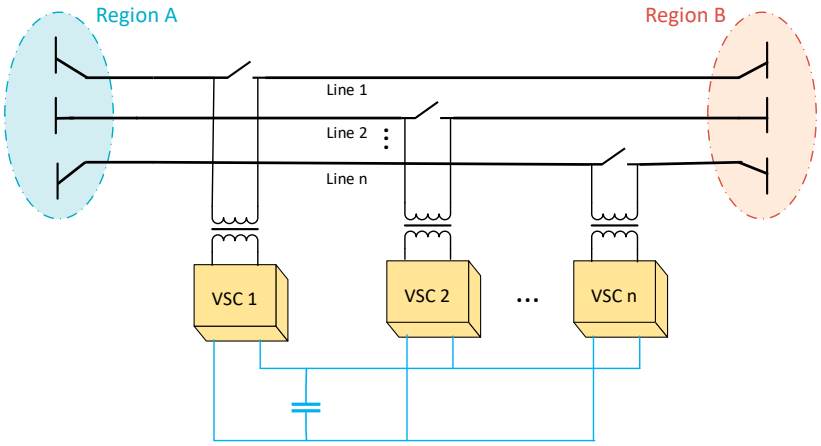

Figure 1. A simplified structure diagram of an IPFC.

In line with other FACTS devices, the IPFC has no exchange of power with the external power system. Instead, it utilizes the shared DC bus of each converter as the focal point for active power exchange to maintain a dynamic balance of power exchange between converters [15–17]. Typically, an auxiliary control line converter has control over only active power or reactive power due to it being primarily accountable for regulating the capacitor voltage of the DC bus, although having full control over both is achievable with a primarily control line converter. Thus, one or more overloaded lines are designated as the primary control lines typically, while the remaining lines are selected as auxiliary control lines.

The depiction of a simplified IPFC equivalent circuit, comprised of two converters, is presented in Figure 2, elucidating the operational characteristics of the IPFC. The voltage amplitude and phase angle of each node are represented by V_i, V_j, V_k, V_m, V_n and θ_i, θ_j, θ_k, θ_m, θ_n respectively. Other symbols in the Figure 2 that represent the parameters of the line can be viewed in Table 1.

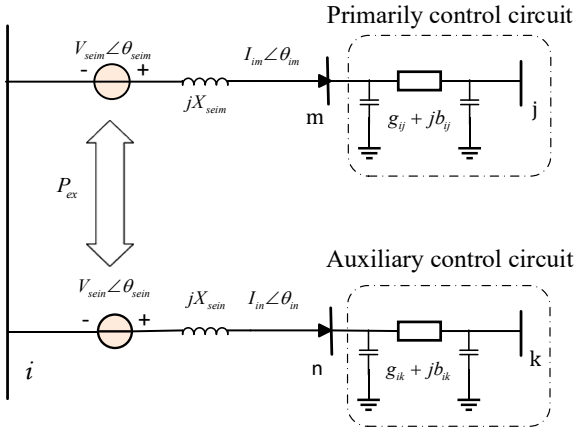

Figure 2. An equivalent circuit diagram of the IPFC.

Table 1. The representation meaning of symbols in Figure 2.

Control Lines	Output Voltage of the Series Transformer	Reactance of the Series Transformer	Equivalent Conductance and Susceptance of the Line	Current
primarily control line (*ij*)	$V_{seim}\angle\theta_{seim}$	X_{seim}	g_{ij}, b_{ij}	$I_{im}\angle\theta_{im}$
auxiliary control line (*ik*)	$V_{sein}\angle\theta_{sein}$	X_{sein}	g_{ik}, b_{ik}	$I_{in}\angle\theta_{in}$

To demonstrate its control characteristics, it was assumed that the two lines were independent of one another while sharing identical parameters. As depicted in Figure 3,

the voltage vector diagram of the primary control line and the voltage compensation line's schematic diagram are presented. The equivalent injection voltage vector was located at the terminus of the $\dot{V}_i$ voltage vector at the line's outset, which could be rotated in a circular motion with a radius equivalent to the maximum injection voltage. The dotted circle denotes the range of the IPFC compensation power. In the diagram, the sending voltage $\dot{V}_i$ was employed as the reference vector, while δ represents the phase difference between the initial voltage and the line's terminal voltage.

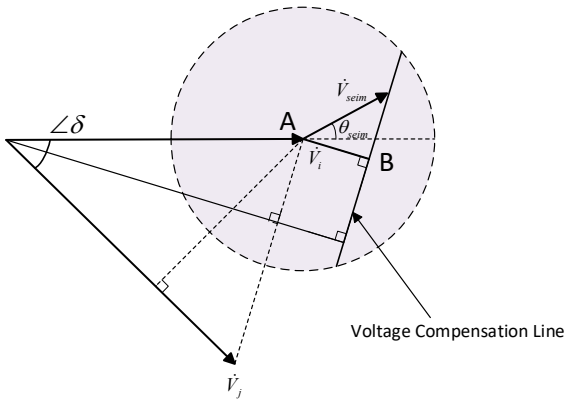

Figure 3. Illustration of voltage compensation line.

To ensure the stable operation of the IPFC, the exchanged active power between the two lines through the DC bus, which was determined through the use of a formula presented in reference [18] in scenarios where the voltage amplitude at the beginning and end of the line was equal, had to satisfy conservation.

$$P_{ex} = \frac{2V_i \sin\left(\frac{\delta}{2}\right)}{X_L} V_{seim} cos\left(\frac{\delta}{2} + \theta_{seim}\right) \quad (1)$$

An analysis of this formula revealed that the active power exchange between the two lines was proportional to $V_{seim} cos\left(\frac{\delta}{2} + \theta_{seim}\right)$, which corresponded to the AB section depicted in Figure 3. Consequently, a voltage compensation line could be defined running parallel to the voltage vector difference between the head and end of the line. If the end of the injected voltage moved along this voltage compensation line, the active power exchange between the two lines would remain unchanged.

The voltage phase difference primarily affects the active power of the line, while voltage amplitude primarily affects its reactive power. By referencing the voltage $\dot{V}_j$ at the line end, the injected voltage can be divided into component V_{seimd} in phase with $\dot{V}_j$ and component V_{seimq} perpendicular to $\dot{V}_j$. This equivalence indicates that the active power of the line is influenced by V_{seimq}, while its reactive power is linked to V_{seimd}. As a result, the reactive power compensation line and the active power compensation line can be obtained. The reactive power compensation line is parallel to the voltage vector $\dot{V}_j$, and when the working point is on the reactive power compensation line, the active power obtained at the power-receiving end remains constant, while the reactive power can be adjusted within a specific range. The active power compensation line reaches a similar outcome.

Figure 4 displays the working vector diagram of the IPFC. The IPFC's equivalent injection voltage operating point on the primary control line is obtained through the intersection of the reactive power compensation line and the active power compensation line. The operating point is confined to a specific voltage compensation line, which is determined by the amount of active power that needs to be exchanged between the lines. Hence, an alteration in the required quantity of the exchanged active power results in a corresponding adjustment of the operating point, shifting from one voltage compensation

line to another. This, in turn, leads to a modification in the active and reactive power of the line, so as to meet the desired power flow. The solid portion of the reactive power compensation line and the active power compensation line in the figure indicates an increase in the corresponding power at the receiving end, while the dotted portion indicates a reduction in the corresponding power at the receiving end.

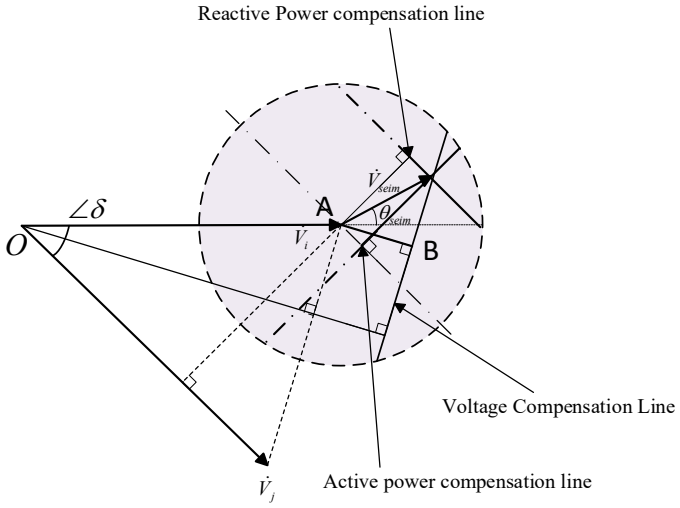

Figure 4. Vector diagram for IPFC.

The IPFC-dynamic-integrated power flow control strategy involves the introduction of a deviation between the active power and reactive power of a line and the target value into the feedback. Upon passing through the controller, typically, the PI controller, mathematical calculation and coordinate transformation, the amplitude and phase angle of the equivalent injection voltage vector $\dot{V}_{seim}$ can be obtained. The amplitude and phase angle of the equivalent injected voltage vector can, subsequently, be introduced into the system to modify the voltage of the power sending end, ultimately achieving the regulation of the line power flow.

In the context of static stability, there is no exchange of power between the IPFC and the external power system, and the active power between each converter is conserved, as demonstrated by the following equation:

$$\mathrm{Re}\left(\dot{V}_{seim}\left(\dot{I}_{im}\right)^{*}\right)+\mathrm{Re}\left(\dot{V}_{sein}\left(\dot{I}_{in}\right)^{*}\right)=0 \tag{2}$$

However, under dynamic control, it becomes necessary to consider the charging and discharging process of the capacitor on the DC bus, which must adhere to the ensuing formula:

$$\mathrm{Re}\left(\dot{V}_{seim}\left(\dot{I}_{im}\right)^{*}\right)+\mathrm{Re}\left(\dot{V}_{sein}\left(\dot{I}_{in}\right)^{*}\right)=C\frac{dV_{dc}}{dt} \tag{3}$$

In the above formula, the line current has the following relationship with the node voltage:

$$\begin{cases} I_{im}\angle\theta_{im}=\frac{(V_i\angle\theta_i+V_{seim}\angle\theta_{seim}-V_m\angle\theta_m)}{jX_{seim}} \\ I_{in}\angle\theta_{in}=\frac{(V_i\angle\theta_i+V_{sein}\angle\theta_{sein}-V_n\angle\theta_n)}{jX_{sein}} \end{cases} \tag{4}$$

3. The Dynamic Droop Control for the IPFC

3.1. Additional Frequency Droop Control Based on the IPFC

IPFC technology allows for the injection of an adjustable voltage vector with a controllable amplitude and phase angle into the power transmission line. As a result, the line flows through the specified active and reactive powers. When the system reaches a steady-

state operation and generates unbalanced power due to disturbances, the IPFC ceases to dynamically control the power flow as the active power flow of the line already achieves the target value. Consequently, the line becomes incapable of responding to frequency fluctuations. In such cases, frequency modulation can solely rely on the capabilities of the uninstalled IPFC line.

To enable IPFC lines to participate in the frequency regulation of the system, an additional frequency control mechanism is introduced based on the IPFC's steady-state operation. The proposed approach involves incorporating the frequency deviation of the system into the target value of the line power flow control. This ensures that the target value of the line power flow can respond to changes in the system frequency. Consequently, the line power flow control quantity changes dynamically following system disturbances, leading to the absorption of unbalanced power in the system and an improvement in system stability. By setting the frequency droop coefficient, the IPFC control target value can follow the system frequency change, thereby facilitating the implementation of additional frequency control based on the IPFC. The mathematical expression for this is formulated as follows:

$$P_{ref}{}^{*} = P_{ref0} + K(f^{*} - f) \tag{5}$$

where $P_{ref}{}^{*}$ represents the target value of the IPFC to control the active power of the line.

P_{ref0} represents the initial target value of line active power, K represents the frequency droop coefficient and f^{*} and f represent the system frequency reference value and the system frequency actual value, respectively.

The degree of line power flow control variation in response to system frequency fluctuations is determined by the droop coefficient of the IPFC. A large frequency droop coefficient results in significant variation in the control of the IPFC on the line power flow, enabling the line to absorb more unbalanced power. Conversely, a small variation in the control of the IPFC on the line power flow results in a reduced ability of the line to absorb unbalanced power. However, fixing the frequency droop coefficient may lead to problems, especially when integrating large-scale renewable energy into the power grid. The unpredictable nature of renewable energy may cause sudden increases or decreases in power generation; in the former case, the IPFC responds to frequency fluctuations via a fixed-frequency droop coefficient, resulting in the target value of the IPFC control line power flow to increase. This may lead to an increased risk of the power flow exceeding the limit when some lines in the system are close to experiencing heavy load.

3.2. Dynamic Droop Control Considering the Line Power Margin

To prevent the occurrence of the power flow exceeding the limit, a dynamic droop control method has been proposed. The proposed method aims to adjust the frequency droop coefficient in a dynamic manner based on the addition of frequency droop control using the IPFC. This method increases the proportion of unbalanced power consumption for lines with large power margins, while ensuring the safety of the lines' operation.

In order to achieve real-time power margin considerations of lines with IPFCs, adaptive rules based on Equation (5) needed to be introduced. When there was a surplus of power in the system and the system frequency increased, the active power flow of each line needed to be increased to maintain a power balance. The power margin of the line with the IPFC corresponded to the difference between the initial active power target value and the maximum allowable active power. Conversely, when the system frequency decreased and the system load suddenly increased, the IPFC-containing lines needed to temporarily reduce the allowable active power to balance the power shortage. The power margin at this point would be the initial active power target value. Finally, the frequency droop control coefficient considering the IPFC power margin was determined using the following equation:

$$K^{*} = \begin{cases} \frac{\alpha K\left(P_{refmax} - P_{ref0}\right)}{P_{refmax}}, f > f^{*} \\ \frac{\alpha K P_{ref0}}{P_{refmax}}, f < f^{*} \end{cases} \tag{6}$$

The frequency droop coefficient, K, was computed using Formula (5) in the aforementioned equation. To account for varying requirements, an adjustment coefficient of $\alpha = 50$ was employed in this study to directly modify the impact of K^* on the line power.

The value of K^* was determined with the power margin of the IPFC line when α was established. Larger power margins resulted in larger K^* values and, thus, greater capacity for the lines to absorb unbalanced power. Conversely, smaller power margins indicated a lower capacity for the lines to absorb unbalanced power, necessitating the prioritization of safe line operations. The control block diagram of an IPFC with dynamic droop control can be viewed in Figure 5. And the symbol $'*'$ in the figure represents multiplication.

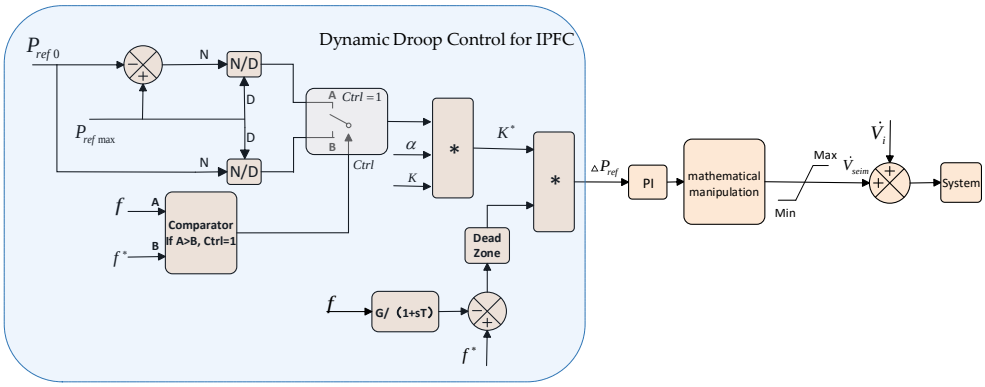

Figure 5. The dynamic droop control for IPFC.

4. Results of Simulation Verification

To assess the efficacy of the suggested additional frequency control method, this study designed three distinct operational scenarios for the simulation analysis: the power target value of the line with the IPFC increased, the load at the sending end of the system was cut off due to a fault and variations in the wind power generation. Table 2 lists the droop controller parameters shown in Figure 5 and the studied system parameters.

Table 2. The parameters of the controller and studied system.

Parameters	Value	Unit
Bus-rated voltage	380	kV
Frequency	50	Hz
DC bus-rated voltage	400	kV
K	120	-
α	50	-
$P_{ref\ max}$	800	MW
Dead zone	$\pm$0.02	Hz

4.1. Simulation Results in Active Power References Increases Scenario

This example aimed to verify the effectiveness of the suggested additional frequency droop control method based on the IPFC, which allowed for the IPFC-installed lines to participate in system frequency regulation and enhance system stability. The experiment involved using line one as the auxiliary control line, and line two, line three and line four as the primarily control lines to regulate the active power at 300 MW, 300 MW and 500 MW, respectively. The IPFC installed on line four was subjected to additional frequency droop control, while no additional frequency droop control was applied to the IPFCs installed on line two and line three.

At 5.5 s, the IPFC increased the active power control value of line three from 300 MW to 700 MW. Figure 6 depicts the response of each electrical quantity in the system. Notably, line two data were not included, as it did not change its active power control value and remained at 300 MW. The system frequency and frequency variation are represented by f

and Δf, respectively. The active power of the lines and their variations are denoted as P_1, P_2, P_3 and P_4 and ΔP_1, ΔP_2, ΔP_3 and ΔP_4, respectively.

Based on the information presented in Figure 6, it was evident that an increase in the IPFC's control power on line three from 300 MW to 700 MW resulted in a decrease in - system frequency, with a maximum of Δf 0.042 Hz. During the new steady-state conditions, the active power was exchanged between the primarily and auxiliary control lines, with line one experiencing a flow of over 400 MW. In case of a disturbance, ΔP_4 amounted to 5.6 MW. It is worth noting that without the use of additional frequency droop control by the IPFC, the system's stability greatly depended on its frequency adjustment ability alone, with line four exhibiting minimal response to any changes in the system's frequency. When the IPFC implemented additional frequency droop control measures, the maximum ΔP_4 was 105 MW, and the maximum Δf was restricted to 0.029 Hz. In this scenario, line four was observed to promptly respond to fluctuations in the system frequency so as to mitigate the frequency deviation through absorbing a portion of the unbalanced power and enhancing the overall stability of the system. Empirical evidence indicated that the introduction of additional frequency droop control measured in the IPFC enabled the line with the IPFC to actively engage in frequency regulation by absorbing unbalanced power, leading to a marked improvement in the stability of the system.

4.2. Simulation Results in Load Variation Scenario

In the initial system state, the primary control and auxiliary control lines were selected as previously described. The active power of line two, line three and line four was controlled at levels of 300 MW, 300 MW and 500 MW respectively, through the IPFC. The IPFC installed on line three and line four applied additional frequency droop control with a fixed-frequency droop coefficient. Meanwhile, the power-sending end, which was directly connected to line three and line four, was connected to a 400 MW load. At 5.5 s, the load at the power-sending end was removed due to a fault, and the response of each electrical quantity of the system can be observed in Figure 7.

Based on the information presented in Figure 7, it was evident that a fault resulting in the removal of a 400 MW load at the power-sending end led to an increase in system frequency, with a maximum Δf of 0.066 Hz. Without additional frequency droop control, each line's active power target value remained stable, and the power flow through the line remained nearly constant. As can be seen, the maximum ΔP_3 and ΔP_4 were 4.6 MW and 4.2 MW, respectively. In such a scenario, line three and line four could not absorb the system's unbalanced power and did not contribute to the system's frequency regulation. However, with additional frequency droop control, the IPFC on both lines increased the active power target value proportionally to the fixed-frequency droop coefficient as the frequency increased. This dynamic control of the line power flow by the IPFC enabled it to absorb the unbalanced power in the system by following the frequency's changes. Given that the frequency droop coefficients were consistent across both lines, the active power increments on the lines were comparable. The maximum active power increments for line three and line four were 122.7 MW and 102.8 MW, respectively. Consequently, the maximum system frequency variation was 0.045 Hz, thereby enhancing its stability. With a reduction in unbalanced power, the generator rotor's unbalanced torque also decreased. Furthermore, Figure 7a demonstrates a decrease in the range of the generator speed change. Therefore, based on the results, the IPFC-based frequency droop control was an effective strategy for addressing fault conditions in the system.

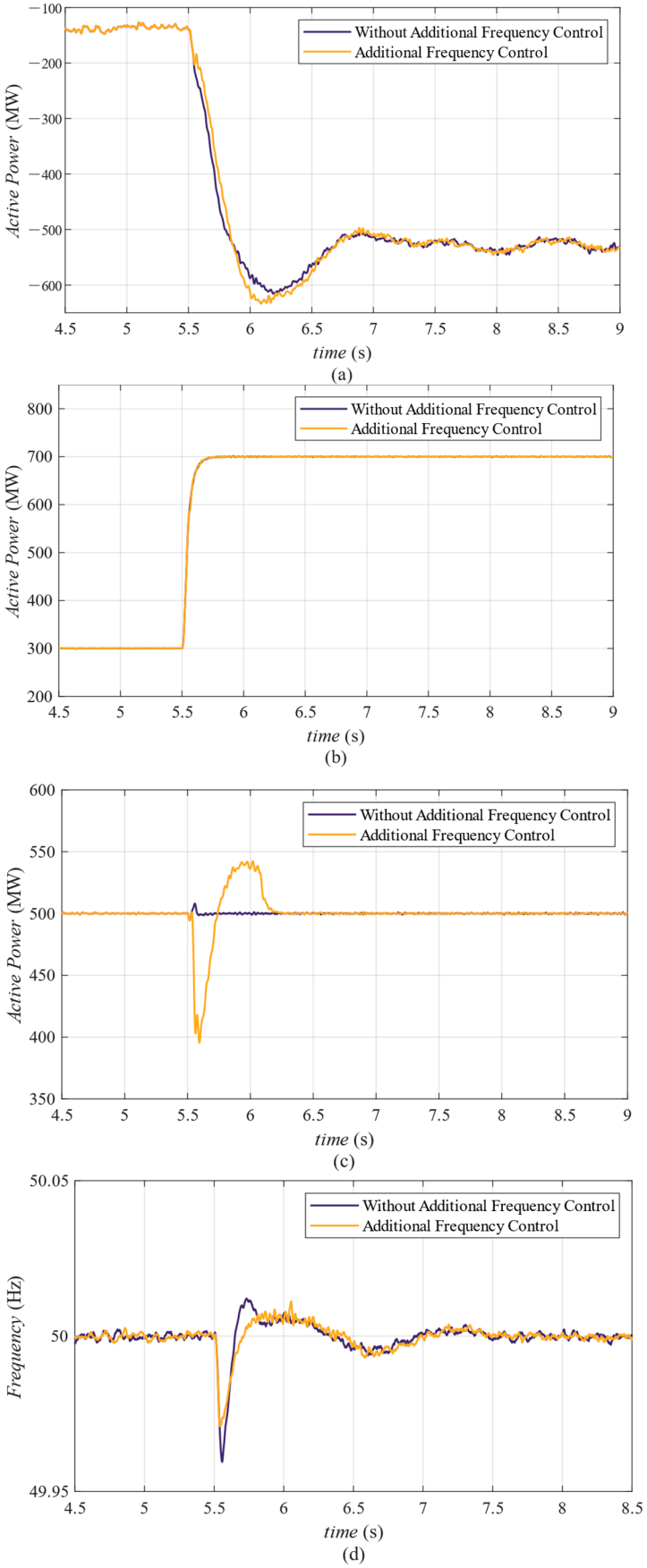

Figure 6. System response when line load increased. (**a**) Active power of line 1; (**b**) active power of line 3; (**c**) active power of line 4; (**d**) system frequency.

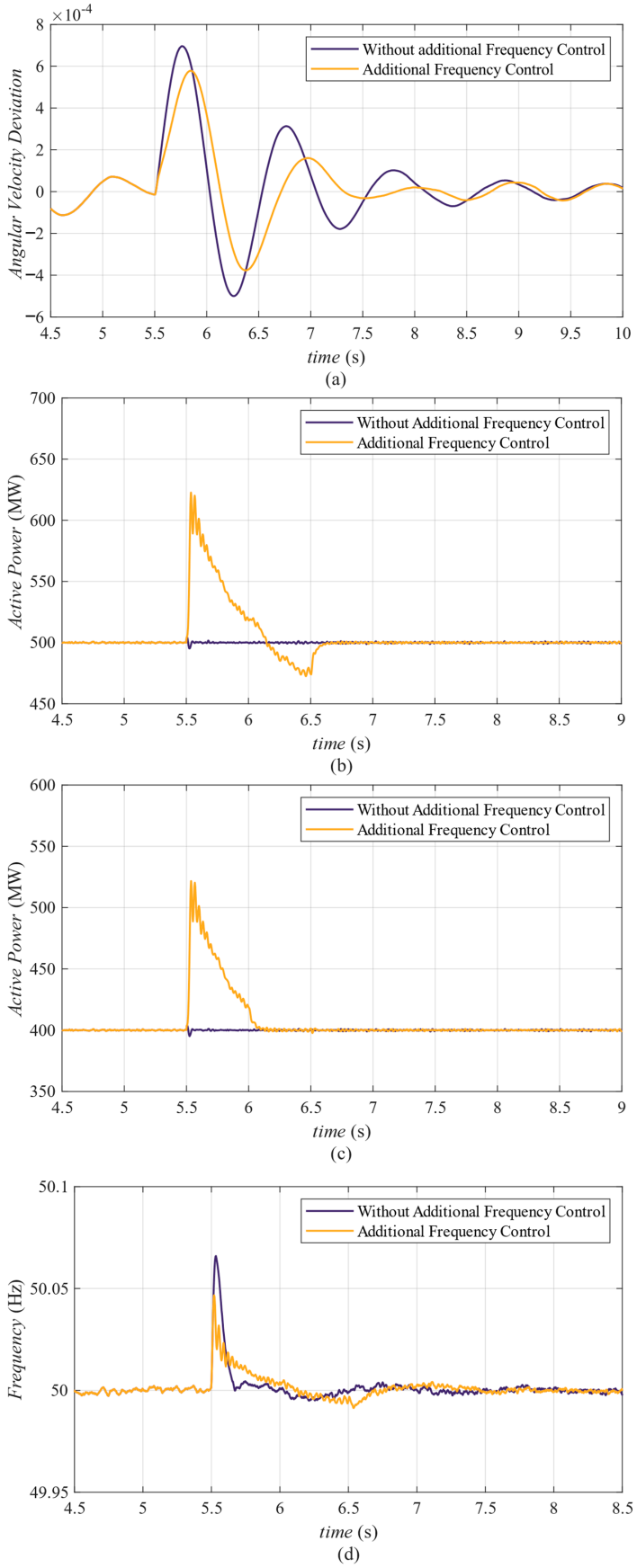

Figure 7. System response when the load at the sending end was removed. (**a**) Generator speed; (**b**) active power of line 3; (**c**) active power of line 4; (**d**) system frequency.

4.3. Simulation Results in Wind Power Fluctuation Scenario

To evaluate the effectiveness of dynamic droop control considering power margins, a comparison was determined with a fixed coefficient additional frequency droop control through this example. The primary and auxiliary control lines were selected as described earlier. Line two, line three and line four controlled the active power at 300 MW, 650 MW and 300 MW, respectively. No additional frequency droop control was applied to the IPFCs installed on line two, while the IPFCs installed on line three and line four utilized dynamic droop control, taking into account the power margin, with a maximum power allowance of 800 MW per line. The initial state saw the wind power connected to the system generating 50 MW, which increased to 550 MW at 5.5 s. The response of each electrical quantity of the system can be viewed in Figure 8.

In its initial state, line three carried 650 MW of power, assigned to the heavy-load line, whereas line four was categorized under the light-load line. It was desirable for line three to not exceed its power flow limit during frequency regulation. According to Figure 8, the system frequency increased with the rise in wind power generation at 5.5 s, with a maximum Δf of 0.083 Hz. Due to there was no additional frequency droop control applied to the IPFC installed on line two, it did not change its active power control value and remained at 300 MW whole time. Additional frequency droop control with a fixed-frequency droop coefficient could be employed to raise the line power flow target value via the IPFC when the frequency increased. As can be seen, the active power was transmitted through line three and line four, with a maximum ΔP_3 of 180.1 MW and a maximum ΔP_4 of 180.9 MW, respectively. By consuming unbalanced power within the system, the frequency variation Δf was reduced to 0.049 Hz, which was lower than the frequency variation observed in the absence of additional frequency droop control. However, due to the IPFC's power flow control, line three's power transmission exceeded 800 MW, resulting in an overload that could hinder the line's safe functioning.

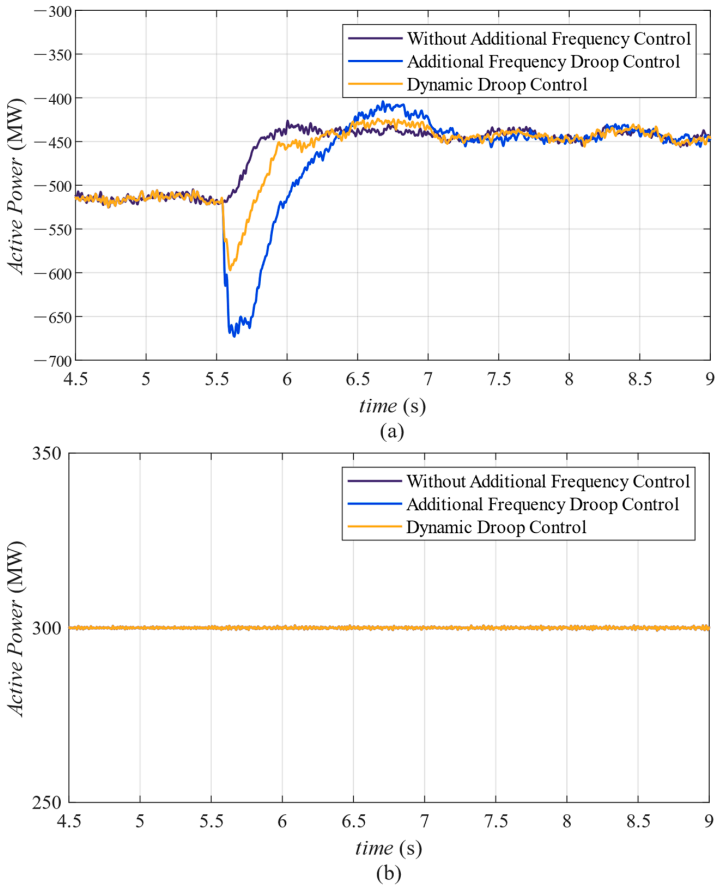

Figure 8. *Cont.*

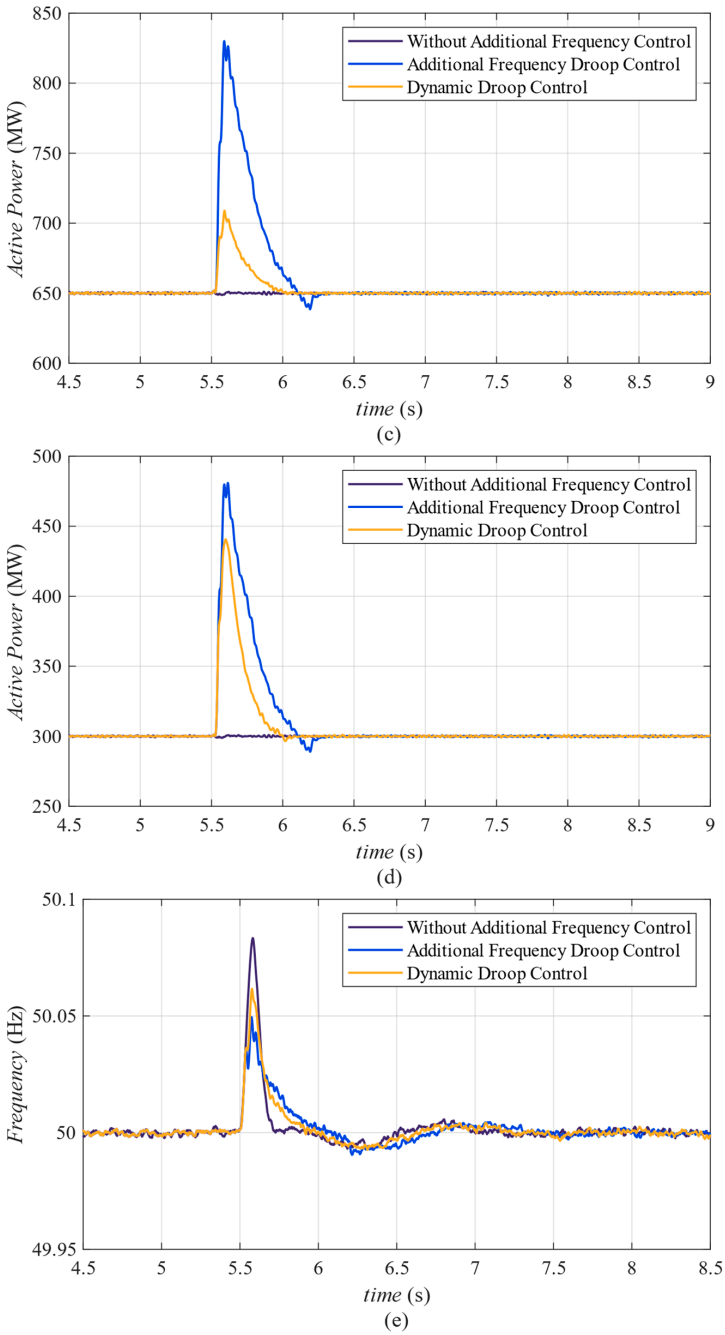

Figure 8. System response when wind power generation increased; (**a**) active power of line 1; (**b**) active power of line 2; (**c**) active power of line 3; (**d**) active power of line 4; (**e**) system frequency.

With the implementation of dynamic droop control that took into account the power margin, when there was an increase in system frequency caused by an increase in wind power generation, the power margin was defined as the difference between the initial active power target value and the maximum allowable active power $P_{refmax} - P_{ref0}$, corresponding to $f > f^*$. In this case, line four exhibited a greater power margin than line three, leading to line four bearing the majority of the unbalanced power in the system. The maximum ΔP_3 and ΔP_4 were 58.9 MW and 140.6 MW, respectively. Additionally, the system frequency variation Δf was 0.061 Hz, which was lower than the variation observed without additional frequency control. These results indicated that the dynamic droop control considering the power margin ensured that the lines with larger power margins bore a greater share of the

unbalanced power during times of system imbalance, thereby maintaining the safety of the heavy-load lines and enhancing system stability.

The initial state of the system remained the same as described earlier. When the wind power generation suddenly dropped from 550 MW to 50 MW at 5.5 s, Figure 9 showcases the response of each electrical component under varying control modes.

According to the information presented in Figure 9, the drop in wind power generation led to a decrease in system frequency, with a maximum Δf of 0.08 Hz. Additional frequency droop control with a fixed-frequency droop coefficient employed in the IPFC caused the power flow target value of line three and line four to decrease when the system frequency decreased. Through the dynamic integrated power flow control strategy of the IPFC, the active power flow of line three and line four changed. The maximum ΔP_3 and ΔP_4 were 195.4 MW and 194.3 MW, respectively. By consuming unbalanced power within the system, the frequency variation Δf was reduced to 0.045 Hz, which was lower than the variation observed without additional frequency droop control. Notably, line two data were similar to the Figure 8b, as there was no additional frequency droop control applied to it, which led to the active power of line two remain at 300 MW whole time.

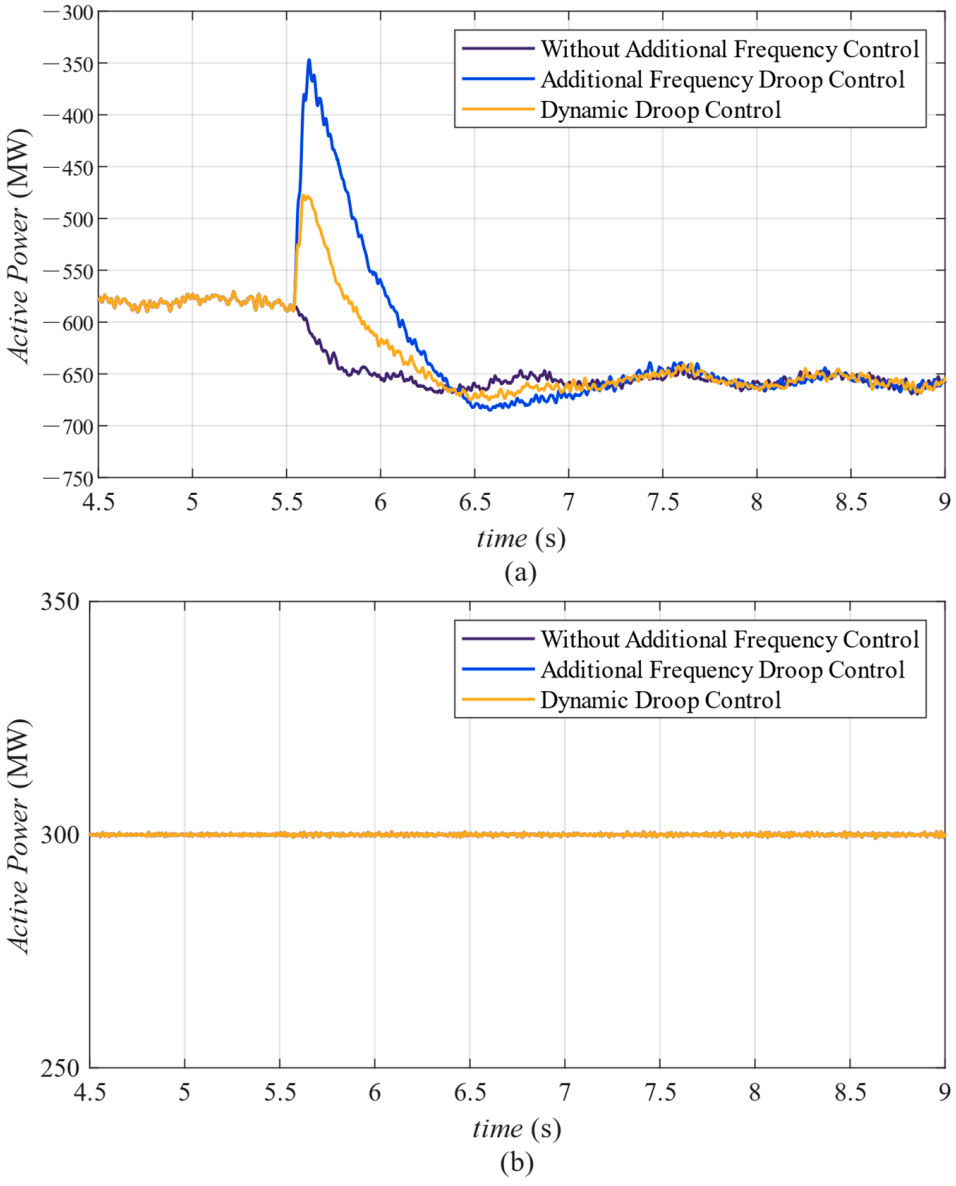

Figure 9. *Cont.*

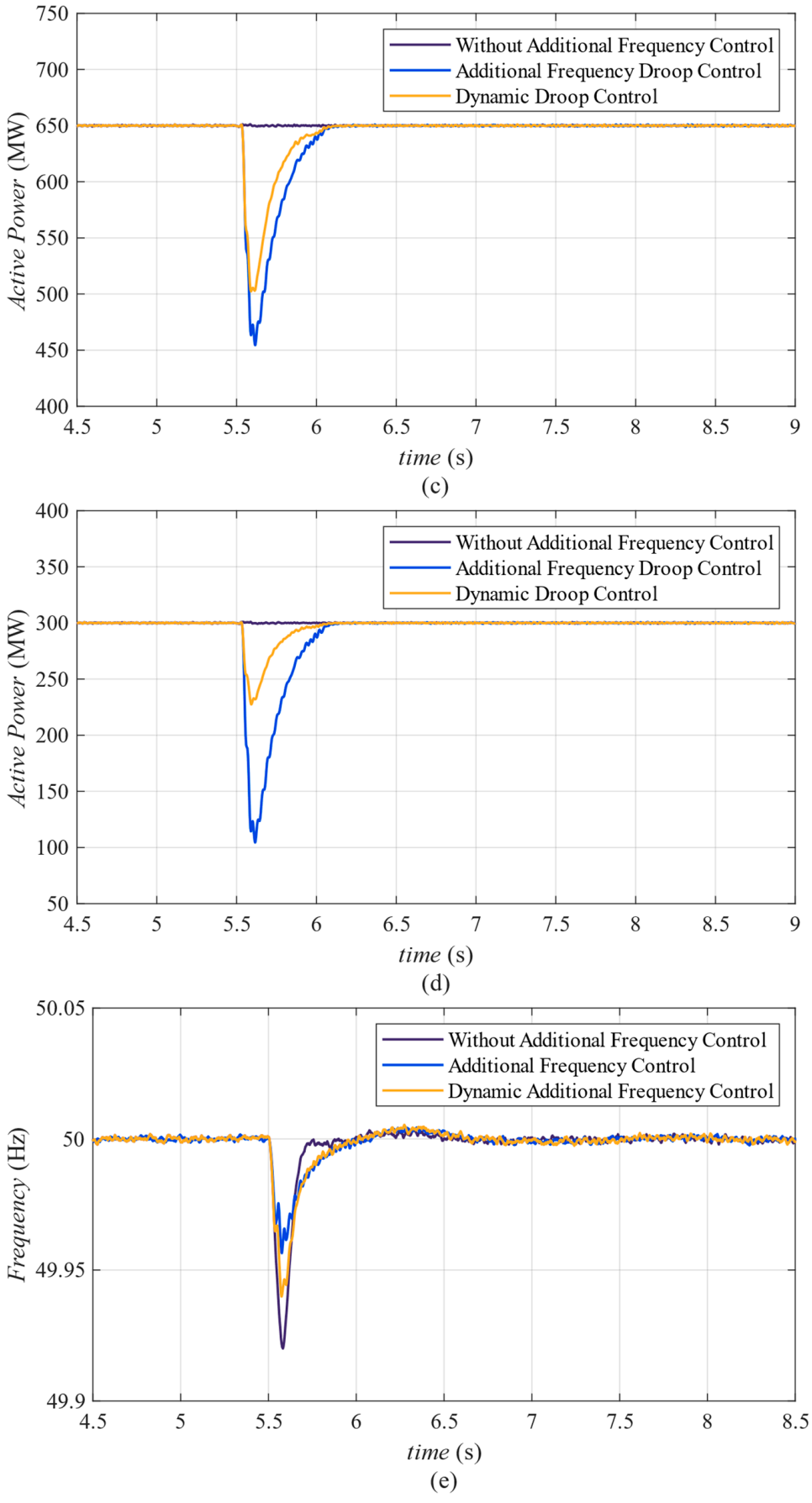

Figure 9. System response when wind power generation decreased; (**a**) active power of line 1; (**b**) active power of line 3; (**c**) active power of line 4; (**d**) active power of line 4; (**e**) system frequency.

With the implementation of dynamic droop control that took into account the power margin, when there was a decrease in the system frequency, the initial active power target value P_{ref0} represented the power margin of the IPFC line. In this case, line three's power margin was greater than that of line four, leading to line three shouldering the majority of the unbalanced power in the system. A comparison of the power variation between the two lines revealed that line three experienced a maximum power variation of 147.7 MW, while line four experienced a maximum power variation of 72.6 MW. The system frequency variation Δf was recorded as 0.058 Hz. The findings demonstrated that the dynamic droop control, which considered the power margin, could effectively enhance the ability of the line to absorb unbalanced power based on the line power margin.

4.4. Comparative Study

An evaluation of the performance of the used control strategies, the IPFC-based power flow control strategy, the IPFC-based additional frequency droop control and the IPFC-based dynamic droop control, was given. Table 3 shows a comparison of the system response under the three control strategies mentioned above when the wind power generation increased, so as to evaluate their control characteristics. These data showed that the IPFC power flow control strategy could retain the power of the installed line as the target value even when there was a significant disturbance, which benefited the improvement of the transmission capacity of the system. The proposed IPFC-based additional frequency droop control strategy resulted in the IPFC lines participating in the frequency regulation of the system. Furthermore, the proposed IPFC-based dynamic droop control could enhance the stability of the system while preventing the line power flow from exceeding the limit.

Table 3. Comparative analysis of the three control strategies.

Parameters	IPFC-Based Power Flow Control Strategy	IPFC-Based Additional Frequency Droop Control Strategy (Proposed)	IPFC-Based Dynamic Droop Control Strategy (Proposed)
The active power variation of line 3	0 MW	180.1 MW (overload)	58.9 MW
The active power variation of line 4	0 MW	180.9 MW	140.6 MW
Frequency variation	0.083 Hz	0.049 Hz	0.061 Hz
The percentage decrease in frequency fluctuation	-	40.96%	26.5%

5. Conclusions

Based on the above theoretical analysis and simulation results, the following main conclusions could be drawn:

(1) By utilizing the IPFC-based additional frequency droop control, a system frequency deviation was introduced into the active power flow control of the line through the IPFC. This allowed the line equipped with the IPFC to absorb the unbalanced power in the system, participate in frequency regulation and effectively reduce the system's frequency deviation.

(2) The dynamic droop control of the IPFC incorporated the power margin of the line into the frequency droop coefficient and adjusted it in real-time based on the operational status of the line. This process ensured that the IPFC line with the larger power margin bore a greater proportion of the unbalanced power, thereby preventing the line power flow from exceeding the limit and improving the overall system stability.

(3) The proposed strategies could be effective in various system operation scenarios. The different simulation results all demonstrated that through the implementation of dynamic droop control, power lines with significant power margins were able to accommodate more unbalanced power, resulting in a reduction in frequency fluctuations caused by disturbances and an enhancement in system stability.

Author Contributions: Conceptualization, C.D., M.W. and B.L.; methodology, C.D., M.W. and B.L.; software, C.D., M.W. and B.L.; validation, C.D., M.W. and B.L.; data curation, C.D., M.W. and B.L.; writing—original draft preparation, M.W.; writing—review and editing, C.D., M.W., T.L. and B.L.; supervision, B.L. and T.L.; project administration, B.L. and Q.J.; funding acquisition, X.L. All authors have read and agreed to the published version of the manuscript.

Funding: This work was supported by the Opening Fund of the Power Internet of Things Key Laboratory of Sichuan province (PIT-F-202208) and was also supported by the General Project of the Natural Science Foundation of Sichuan province (2022NSFSC0262).

Data Availability Statement: Not applicable.

Conflicts of Interest: The authors declare no conflict of interest.

References

1. Mahmoud, M.M.; Atia, B.S.; Esmail, Y.M.; Ardjoun, S.A.E.M.; Anwer, N.; Omar, A.I.; Alsaif, F.; Alsulamy, S.; Mohamed, S.A. Application of Whale Optimization Algorithm Based FOPI Controllers for STATCOM and UPQC to Mitigate Harmonics and Voltage Instability in Modern Distribution Power Grids. *Axioms* **2023**, *12*, 420. [CrossRef]
2. Abdel Mohsen, S.E.; Ibrahim, A.M.; Elbarbary, Z.M.S.; Omar, A.I. Unified Power Quality Conditioner Using Recent Optimization Technique: A Case Study in Cairo Airport, Egypt. *Sustainability* **2023**, *15*, 3710. [CrossRef]
3. Li, G.-Q.; Li, S.; Li, X.-J. Available Transfer Capability Calculation Considering FACTS Controllers. *Proc. CSEE* **2009**, *29*, 36–42.
4. Zhang, N.; Liu, J.; Chen, J.; Yao, Y.; Bao, Y.; Chen, P.; Zhou, X. Low Frequency Oscillation Suppression Method Based on Flexible Load and UPFC. *Dianli Xitong Baohu Yu Kongzhi/Power Syst. Prot. Control.* **2019**, *47*, 82–87. [CrossRef]
5. Zhang, S.; Wang, T.; Gu, X.; Qin, X. Power Grid Homogeneous Dispatch Based on Transmission Topology Optimization. *Dianwang Jishu/Power Syst. Technol.* **2017**, *41*, 2957–2963. [CrossRef]
6. An, S.; Condren, J.; Gedra, T.W. An Ideal Transformer UPFC Model, OPF First-Order Sensitivities, and Application to Screening for Optimal UPFC Locations. *IEEE Trans. Power Syst.* **2007**, *22*, 68–75. [CrossRef]
7. Cui, Y.; Yu, Y.; Bao, W.; Feng, Y.; Guo, Q.; Xie, W.; Jin, M. Analysis of Application Effect of 220 KV UPFC Demonstration Project in Shanghai Grid. *J. Eng.* **2019**, *16*, 758–762. [CrossRef]
8. Cai, H.; Yang, L.; Wang, H.; Song, P.; Xu, Z. Application of Unified Power Flow Controller (UPFC) in Jiangsu Power System. In *2017 IEEE Power & Energy Society General Meeting*; IEEE: Piscatway, NJ, USA, 2017; p. 89.
9. Wu, X.; Wang, L.; Chen, X.; Liu, Y.; Tao, J.; Xu, X.; Chen, X. Optimal Power Flow Considering Interline Power Flow Controller. *Dianwang Jishu/Power Syst. Technol.* **2019**, *43*, 4125–4132. [CrossRef]
10. Zhu, L.; Yuan, Z.; Chao, S.H.E.N.G. Review of Frequency Support Control Methods for Asynchronous Inter-Connection System Based on VSC-HVDC. *Electr. Power Autom. Equip.* **2019**, *39*, 84–92.
11. Chaudhuri, N.R.; Majumder, R.; Chaudhuri, B. System Frequency Support through Multi-Terminal DC (MTDC) Grids. *IEEE Trans. Power Syst.* **2012**, *28*, 347–356. [CrossRef]
12. Dai, J.; Phulpin, Y.; Sarlette, A.; Ernst, D. Coordinated Primary Frequency Control among Non-Synchronous Systems Connected by a Multi-Terminal High-Voltage Direct Current Grid. *Iet Gener. Transm. Distrib.* **2012**, *6*, 99–108. [CrossRef]
13. Zhu, J.; Booth, C.D.; Adam, G.P.; Roscoe, A.J.; Bright, C.G. Inertia Emulation Control Strategy for VSC-HVDC Transmission Systems. *IEEE Trans. Power Syst.* **2013**, *28*, 1277–1287. [CrossRef]
14. Wang, R.; Chen, L.; Zheng, T.; Mei, S. VSG-Based Adaptive Droop Control for Frequency and Active Power Regulation in the MTDC System. *CSEE J. Power Energy Syst.* **2017**, *3*, 260–268. [CrossRef]
15. Mohamed, K.H.; Rao, K.R.; Hasan, K.N.B.M. Optimal Parameters of Interline Power Flow Controller Using Particle Swarm Optimization. In *2010 International Symposium on Information Technology*; IEEE: Piscatway, NJ, USA, 2018; pp. 727–732.
16. Wang, L.; Wu, X.; Chen, X.; Liu, Y.; Tao, J.; Xu, X.; Chen, X. Step by step Site Selection and Multi objective Optimal Capacity of Interline Power Flow Controller. *Power Capacit. React. Power Compens.* **2019**, *40*, 6. [CrossRef]
17. Reddy, B.R.; Reddy, Y.S.; Sujatha, P. Optimal Placement of Interline Power Flow Controller (IPFC) to Enhance Voltage Stability. In Proceedings of the 2015 Conference on Power, Control, Communication and Computational Technologies for Sustainable Growth (PCCCTSG), Kurnool, India, 11–12 December 2015; IEEE: Piscatway, NJ, USA, 2015; pp. 78–84.
18. Chen, J.; Lie, T.T.; Vilathgamuwa, D.M. Basic Control of Interline Power Flow Controller. In Proceedings of the 2002 IEEE Power Engineering Society Winter Meeting. Conference Proceedings (Cat. No. 02CH37309), New York, NY, USA, 27–31 January 2002; IEEE: Piscatway, NJ, USA, 2002; pp. 521–525.